(Received 19 June 2025, Accepted 5 August 2025, Scheduled 14 August 2025)

Reconfigurable Flexible Hybrid Antenna for Body Area Networks

Bendalam Alekhya[1, 2, *] and Anjaneyulu Lokam[1]

[1] *Department of Electronics and Communication Engineering, National Institute of Technology Warangal, Telangana, India*
[2] *Department of Electronics and Communication Engineering VNR Vignana Jyothi Institute of Engineering and Technology Hyderabad, Telangana, India*

ABSTRACT: This paper presents a simple liquid crystal polymer (LCP) substrate material-based frequency and pattern reconfigurable antenna for body-centric communication applications. The designed antenna is circular in shape with multiple spars in the radiating element. PIN diodes are arranged on either side of the lower portion at the concentric circular arc of the feed line for external switching. The upper portion of the radiating structure is connected with inductor and capacitor for proper impedance matching to attain the desired band of frequency. The constructed LCP substrate-based antenna is flexible in nature and conformal to the congregation surface in body area network applications. Frequency reconfigurability with switching between PCS (1.8–1.9 GHz) to WLAN (5.1–5.3 GHz) and ISM band (5.7–5.8 GHz) makes the model more appropriate for wearable applications with low specific absorption rate (SAR) less than 1.6 w/kg, which is in the standards. Additionally, the projected design demonstrates pattern reconfigurability with a 30-degree tilt at different switching conditions.

1. INTRODUCTION

The demand for reconfigurable antennas is growing tremendously due to their adaptable nature as per the spontaneous requirements in communication systems. Hybrid reconfigurability is preferred over either one to attain multiple benefits and to switch in accordance with the situation in demand. Frequency-reconfigurable antennas can provide switching between operating bands only, but the combination of pattern and polarization reconfigurability [1, 2] makes them more useful and powerful with multiple advantages. This can be attained by varying the impedance, dielectric constant of the substrate, orientation of surface current, etc. [3, 4]. Research is progressing with different substrate materials, diodes, and advanced switches to attain reconfigurability in the designed antennas. Several successful models are available in the literature, which are suitable for commercial communication applications. The antenna models with flexibility and reconfigurability for off-body communication applications need to be analyzed for future wearable communication applications [5–7].

A few works that are reported in the literature using PIN diodes to achieve frequency and pattern reconfigurability are summarized here. A bowtie antenna with two arms printed on either side of the substrate to attain the frequency re-configurability for WiMAX and WLAN applications is reported in [8–10]. A button-shaped pattern reconfigurable wearable antenna is presented for industrial, scientific, and medical (ISM) band applications operating at 2.45 GHz in [11]. This antenna is loaded with inductance to change the zeroth order response and provides resonant frequencies at two switching conditions. An inkjet printed reconfigurable antenna printed on a paper substrate operating at 1.9 GHz and 2.4 GHz using PIN diodes is presented in [12]. U-shaped stubs are employed on either side of the radiating patch to obtain additional operating bands. A pattern reconfigurable antenna with four arc-shaped dipoles with broadband feeding network is presented in [13]. To attain pattern reconfigurability, quarter wave transformer and broad balun with L-shaped feedline are introduced with arc dipoles at 90°. By connecting PIN diode switches in between the arc dipoles, reconfigurability is achieved with different switching combinations. A planar reconfigurable antenna with pattern switching is presented in [14] using a Wilkinson power divider attached to feeding port and inverted trident at the bottom layer. A dual reconfigurable monopole antenna for USB dongle applications is presented in [15] to access 3G/4G networks. To attain frequency switching, a switch is connected across a mender line and rectangular strip to vary the electrical length of the antenna. A rectangular patch antenna with Koch fractal is presented in [16, 17] to obtain the reconfigurable characteristics.

2. ANTENNA DESIGN

The antenna design using a liquid crystalline polymer (LCP) substrate (Rogers ULTRAM 3850) with different iterations is shown in Fig. 1. A basic circular monopole antenna is designed with coplanar waveguide (CPW) feeding and later it has been modeled to an annular ring structure as shown in Fig. 1(a) and Fig. 1(b). Vertical strips are arranged around the inner part of the annular ring as shown in Fig. 1(c), and thereafter central slot is placed as shown in Fig. 1(d) with a defected ground structure

* Corresponding author: Bendalam Alekhya (alekhya_v@vnrvjiet.in).

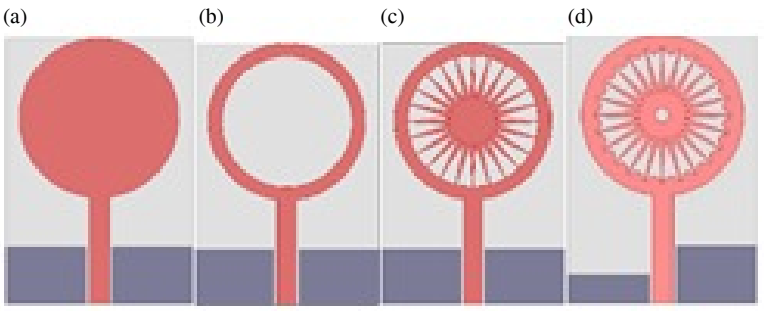

FIGURE 1. Antenna modelling. (a) Basic circular patch (Ant 1). (b) Modeled annular ring (Ant 2). (c) Integrated Spokes (Ant 3). (d) Proposed antenna with DGS.

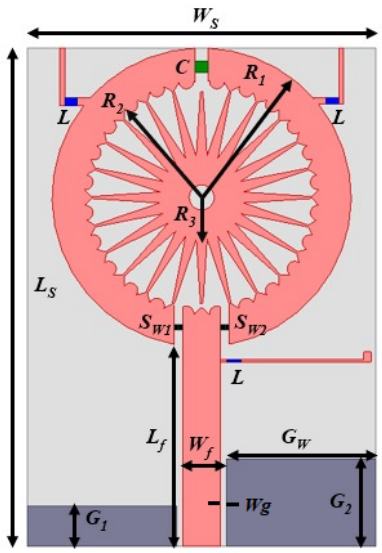

FIGURE 2. Proposed antenna with reconfigurability arrangement ($W_s = 28$, $L_s = 40$, $W_g = 0.2$ mm, $W_f = 3$ mm, $L_f = 17$ mm, $R_1 = 9$ mm, $R_2 = 7$ mm, $R_3 = 3.5$ mm, $G_w = 12.3$ mm, $G_1 = 4$ mm, $G_2 = 8$ mm).

(DGS). The arrangement is made in such a way that the partial ground and antenna structure provide a good impedance matching. A detailed structure of the proposed antenna is shown in Fig. 2 with arrangement for reconfigurability with switches (Model BAR64-03V), inductors, and capacitor added for the purpose of DC biasing to the switches.

The radius R_1 is calculated using the equation

$$R_1 = \frac{F}{\left\{1 + \frac{2h}{\pi\varepsilon_r}\left[\ln\left(\frac{\pi F}{2h}\right) + 1.7726\right]\right\}^{1/2}} \quad (1)$$

where

$$F = \frac{8.791 \times 10^9}{f_r\sqrt{\varepsilon_r}} \quad (2)$$

The resonant frequency is 'f_r', relative permittivity 'ε_r' (2.1), effective relative permittivity 'ε_{eff}', and 'h' (0.1 mm) is the thickness of the substrate. The effective outer and inner radii are R_{1eff} and R_{2eff}

$$\varepsilon_{eff} = 0.5\left(\varepsilon_r + 1\right) + 0.5\left(\varepsilon_r - 1\right)\sqrt{\left(1 + 10t/W\right)} \quad (3)$$

$$R_{1eff} = R_1 + 0.5\left(W_{eff}(f) - W\right) \quad (4)$$

$$R_{2eff} = R_2 - 0.5\left(W_{eff}(f) - W\right) \quad (5)$$

where

$$W_{eff}(f) = W + \left(W_{eff}(0) - W\right)/\left(1 + (f/f_p)^2\right) \quad (6)$$

$$W_e(0) = {}^{120\pi t}/_{z_0\sqrt{\varepsilon_e}} \quad (7)$$

$$f_p = z_0/(2\mu_0 t) \quad (8)$$

μ_0 is the permeability, and z_0 is the quasi-static characteristic impedance of a circular ring.

A CPW feed is carefully designed to ensure proper impedance matching and efficient signal transmission. The gap between the signal line and ground planes, which is a critical parameter in CPW design, was optimized through parametric analysis. In the design, the gap dimension is 0.2 mm, and the signal strip width is 3 mm, which together are chosen to achieve a characteristic impedance of 50 ohms. These values were determined based on standard CPW impedance equations and confirmed through simulation to ensure minimal reflection and high return loss.

The dimensions mentioned in Fig. 2 are all optimized through parametric study. The upper portion of the circular ring and the lower portions near the feed line are cut down with slots. The upper edges are connected with slits and inductors, and the upper middle cut is connected with a capacitor. Two PIN diode switches are connected between lower part junctions at feedline and attached an additional inductance based slit also to tune the antenna impedance characteristics. The vertical strips incorporated within the proposed antenna design are pivotal in augmenting its electromagnetic attributes. Specifically, these strips fulfil the following functions:

Impedance Matching: The vertical strips facilitate the tuning of the antenna's input impedance, which results in enhanced impedance matching across the targeted frequency bands, thereby optimizing return loss and overall operational efficiency.

Resonance Control: Through the alteration of the current distribution on the radiating surface, the vertical strips assist in the establishment of additional resonance modes or the alteration of existing resonance frequencies. This characteristic is especially advantageous for realizing multi-band or wideband functionality.

Current Path Extension: The strips effectively augment the electrical length of the antenna without a substantial increase in its physical dimensions, which aids in miniaturization and accommodates lower-frequency operations.

Radiation Pattern Improvement: The incorporation of vertical strips can affect the flow of surface currents and assist in stabilizing or shaping the radiation pattern, yielding more favorable directional characteristics or enhanced gain.

The parameters of the inductor (L) and capacitor (C) utilized in conjunction with the PIN diode are meticulously determined in accordance with the operational frequency of the antenna and requisite biasing conditions. The value of the inductor is specifically selected to yield a high impedance at the designated operating frequency, thereby efficiently isolating the radio frequency (RF) signal from the direct current (DC) bias pathway. In a similar fashion, the value of the capacitor is chosen to present a low impedance at RFs, thereby facilitating the transmission of the signal while simultaneously obstructing DC. These parameters were computed with careful consideration of resonance phenomena, impedance characteristics, and the practical availability of surface-mount components. The ascertained impedance values guarantee that the PIN diode operates effectively without compromising the performance of the antenna. This arrangement guarantees the requisite switching characteristics while preserving impedance matching and radiation efficiency. The components selected underwent rigorous validation through both simulation analyses and experimental confirmation.

PIN diode ON State Resistance $(Rs) = 0.85\,\Omega$ to $1\,\Omega$, and OFF State Resistance $(R) = 2\,\text{k}\Omega$ to $20\,\text{k}\Omega$.

Capacitance $(C) = 0.01$ pF to 0.5 pF, and Inductance $(L) = 0.4$ nH to 0.7 nH.

To achieve adequate impedance matching throughout the various reconfigured states, the antenna's geometric configuration was meticulously optimized, and passive components (including inductors and capacitors) were judiciously incorporated. The impedance matching network is composed of a synthesis of these lumped elements alongside the structural components of the antenna, collectively ensuring a return loss surpassing -10 dB across all operational states. Moreover, comprehensive full-wave electromagnetic simulations were executed to validate the impedance matching across each configuration, with results affirming consistent and efficient operational performance.

The design under consideration has been developed with careful attention to a synthesis of performance criteria, domain-specific requirements, and the benefits conferred by the selected configuration. In particular, the design aspires to attain a compact form factor, reconfigurability, and superior radiation characteristics, which are imperative for contemporary wireless and wearable communication technologies.

The incorporation of attributes such as PIN diode-based switching, optimized geometric configurations, and ancillary passive components (inductors and capacitors) facilitates frequency and/or pattern reconfigurability. This adaptability empowers the antenna to accommodate various operational frequency bands, thereby rendering it suitable for multiband utilization. Moreover, the structural framework was deliberately selected to preserve optimal impedance matching, high efficiency, and acceptable specific absorption rate (SAR) values in proximity to the human body.

3. RESULT ANALYSIS

Ansys HFSS simulator tool has been used to design and study the performance characteristics. Fig. 3 shows the simulated reflection coefficient (in dB) characteristics of the antenna at different iterations (as shown in Fig. 1) during the development. The antenna exhibits dual bands and resonates at 2.5 GHz with bandwidth of 0.9 GHz and at 5.8 GHz with 1.2 GHz bandwidth.

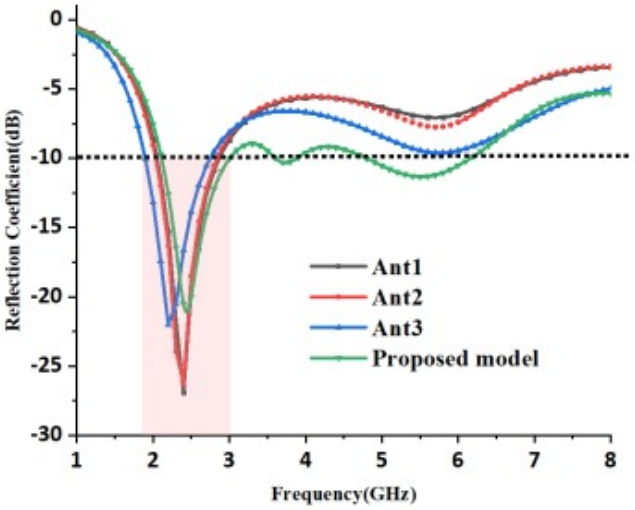

FIGURE 3. Reflection coefficient characteristics of the antenna at different iterations.

The surface current distribution for the four switching conditions are presented in Fig. 4. When botch switches are in OFF condition, the surface current is concentrated at feed line and nearby ground plane. When switches are in OFF, ON (SW_1, SW_2) condition, the surface current is concentrated at lower part of feed line and spokes. When switches are in ON, OFF (SW_1, SW_2) condition, the lower part of spokes, feed line, and circular patch participate in the radiation. When both the switches are in ON condition, the radiation is little bit low and concentrated at edges of the feed line.

Figure 5 shows the three-dimensional radiation characteristics of the antenna for the four different switching conditions. It can be observed that the antenna radiation direction is getting switched, and hence pattern reconfigurability is achieved.

The fabricated prototype antenna is tested in an anechoic chamber, and the measurement setup is shown in Fig. 6. Biasing circuit is designed and connected to antenna with power supply arrangement. The reflection coefficient is measured for the four switching conditions and recorded. The measurements very closely agree with the simulation results, thus validating the design. The change in operating bands and their bandwidths are shown in Fig. 7 for these four switching conditions, and the observed values are given in Table 1. The switching combinations thus provide the frequency reconfigurability simultaneously.

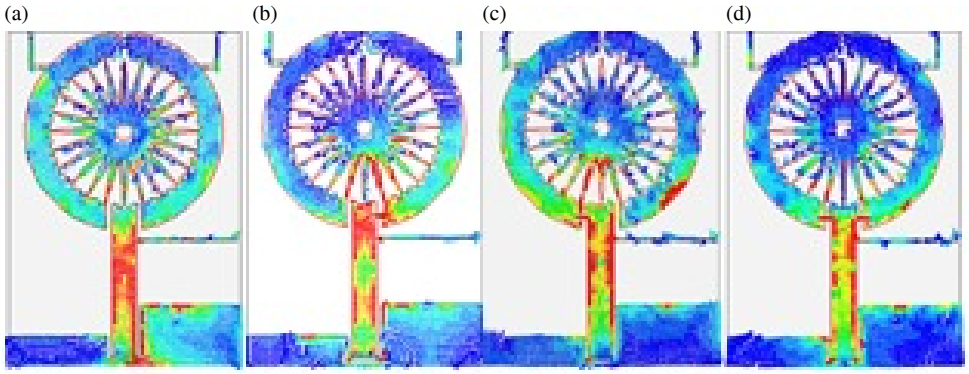

FIGURE 4. Surface current at four switching positions. (a) SW_1 = OFF, SW_2 = OFF, (b) SW_1 = OFF, SW_2 = ON, (c) SW_1 = ON, SW_2 = OFF, (d) SW_1 = ON, SW_2 = ON.

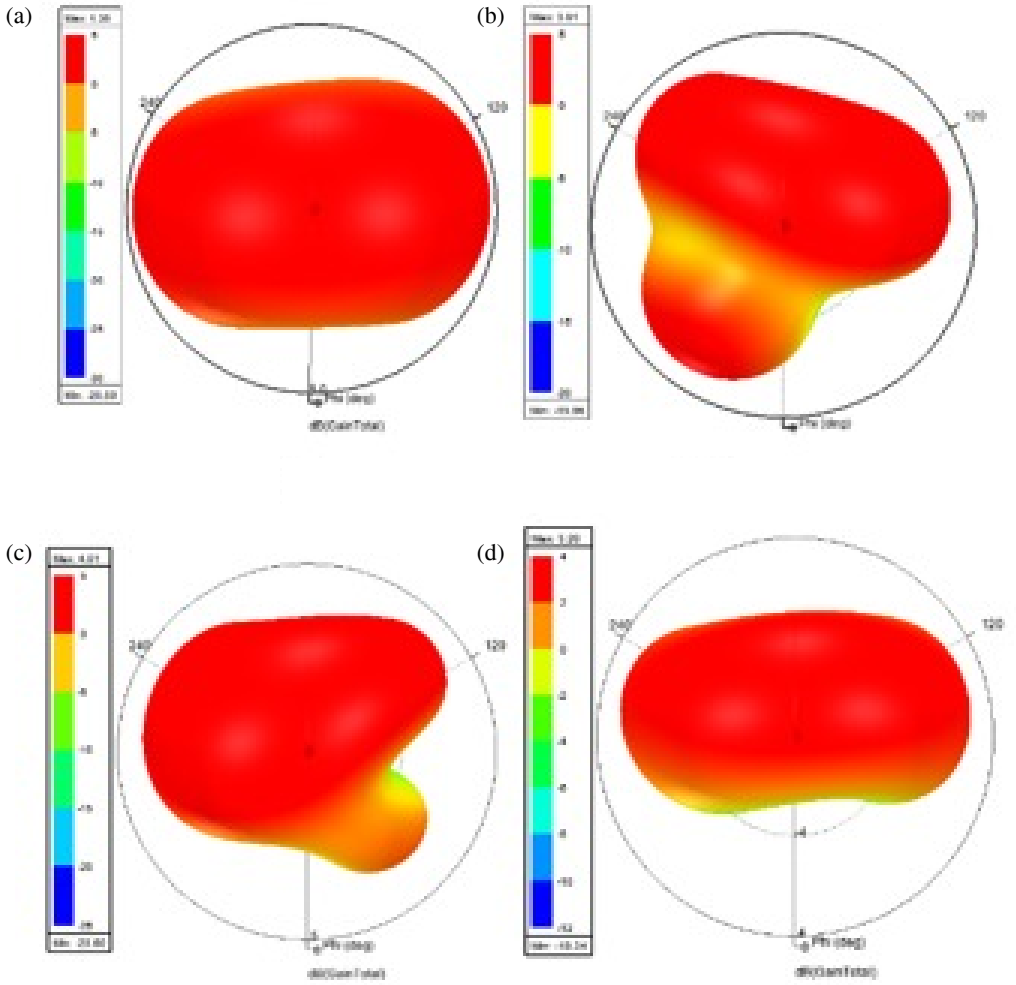

FIGURE 5. Three-dimensional pattern reconfigurability for switching positions of ON and OFF in Simulation. (a) SW_1 = OFF, SW_2 = OFF (b) SW_1 = OFF, SW_2 = ON (c) SW_1 = ON, SW_2 = OFF (d) SW_1 = ON, SW_2 = ON.

The radiation efficiency is also measured and presented for all switching conditions in Fig. 8. The results are in very good agreement with the simulation results providing the experimental validation. The gain is varied between 3.2 and 4.8 dBi in the operating bands, and the peak value is 3.5.

4. SPECIFIC ABSORPTION RATE (SAR) ANALYSIS

In SAR (Specific Absorption Rate) analysis, a multi-layered human tissue model was considered to replicate realistic body conditions. The following average anatomical thicknesses were used based on standard biomedical references:

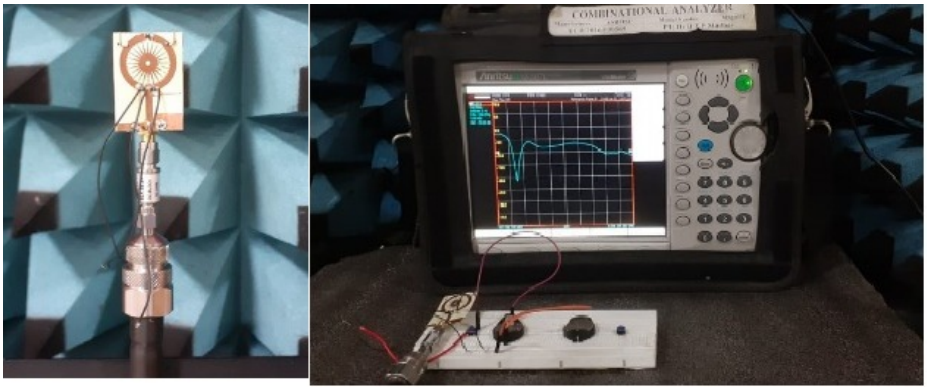

FIGURE 6. Measurement in anechoic chamber with VNA.

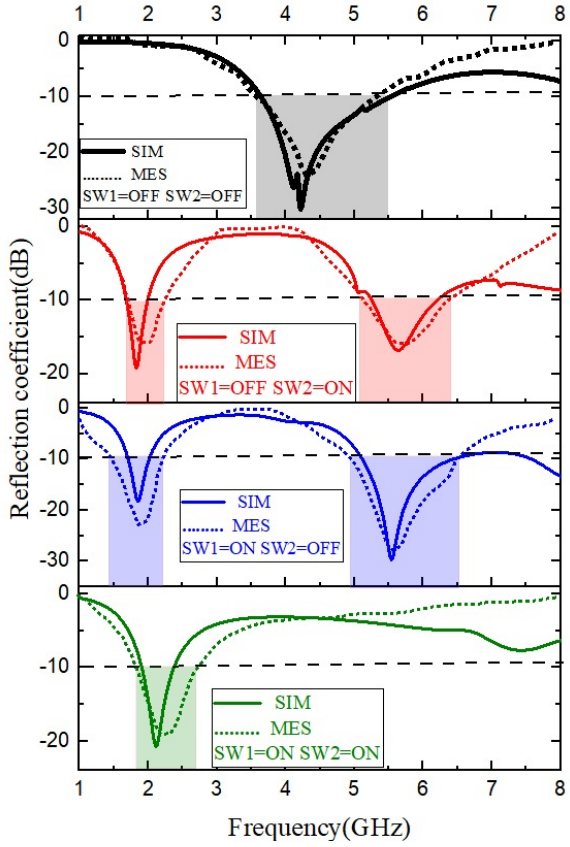

FIGURE 7. Reflection coefficient (S_{11}) for different switching conditions.

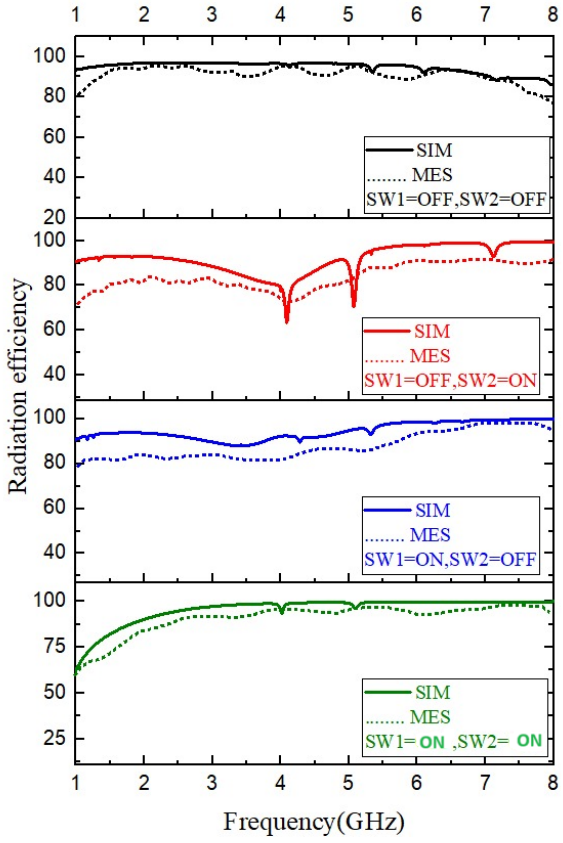

FIGURE 8. Efficiency of the antenna at different switching positions of ON and OFF.

- Skin thickness: 2 mm
- Fat layer thickness: 5 mm
- Muscle layer thickness: 20 mm

These values are used in SAR simulations to assess electromagnetic absorption accurately in this work.

A human phantom body has been imported to an electromagnetic tool, and the antenna is placed on the phantom model as shown in Fig. 9. The compatibility-based testing analysis has been performed, and the results obtained are presented in the SAR analysis section below.

4.1. SAR Analysis

The specific absorption rate analysis has been carried out with the antenna operating at different bands under four switching conditions, and SAR variation is shown in Fig. 10. The results show the satisfactory values of SAR below 1.6 w/kg as per the SAR standards.

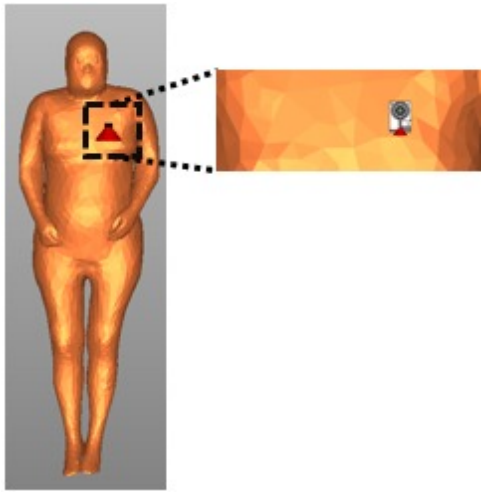

FIGURE 9. Position of the proposed antenna on the human phantom model.

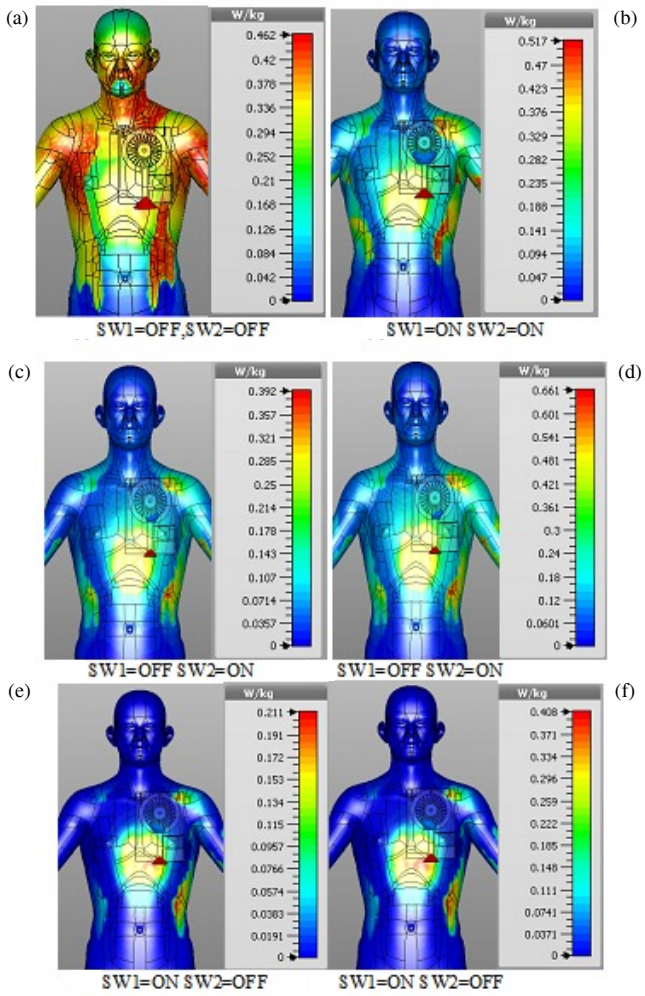

FIGURE 10. SAR analysis of antenna at different switching condition. (a) 4.1 GHz, (b) 2.1 GHz, (c) 1.8 GHz, (d) 5.6 GHz, (e) 1.8 GHz, (f) 5.5 GHz.

Far-field radiation pattern analysis is presented in Fig. 11 for four switching conditions and operating bands. Both XY and

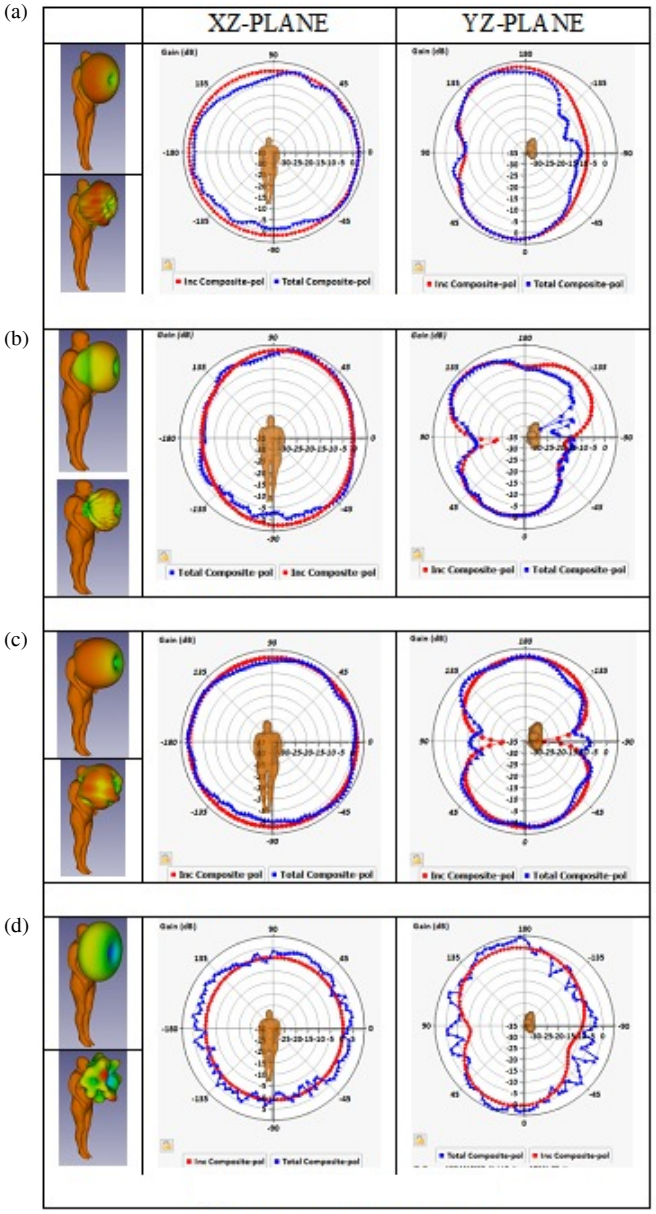

FIGURE 11. Far-field radiation patterns on the human body. (a) SW_1 = OFF, SW_2 = OFF at 4.1 GHz. (b) SW_1 = OFF, SW_2 = ON at 1.8 GHz. (c) SW_1 = OFF, SW_2 = ON at 5.6 GHz. (d) SW_1 = ON, SW_2 = ON at 2.1 GHz.

YZ planes are considered for radiation pattern studies in polar and 3D views. Monopole like and omnidirectional patterns are obtained in E- and H-planes. The co-pol pattern exhibits strong directional lobes, indicating efficient radiation in desired directions. The cross-pol components are significantly lower in magnitude than the co-pol one ensuring the polarization purity. The slight variations noticed in the co-pol and cross-pol patterns are possibly due to fabrication and measurement tolerances, imperfections in the test setup, or environmental reflections. The radiation pattern shows multiple lobes, suggesting a complex antenna structure or multi-mode radiation behavior and maintains reasonable symmetry, indicating good design and consistent antenna behavior across the measured plane.

TABLE 1. Operating bands for different switching positions.

Switching condition		Working frequency bands (GHz)		Impedance bandwidth (%)	
SW_1	SW_2	Sim	Meas	Sim	Meas
OFF	OFF	3.5–5.5	3.5–5.4	44	43
OFF	ON	1.69–1.9 5.2–6.2	1.7–2.2 5.0–6.6	16 16	25 26
ON	OFF	1.72–2.10 5.12–6.14	1.6–2.2 5.1–6.18	19 18	31 19.2
ON	ON	1.8–2.3	1.7–2.8	26	44

TABLE 2. Comparison with pervious literature.

Ref	Dimensions (mm x mm x mm)/ Substrate	Operating Frequency GHz	Impedance Bandwidth (%)	No. of Diodes used	Gain (dBi)	Reconfiguration	Technique used
[1]	42 × 38 × 1.5 FR4	1.9–11	165	4 HPND-4005	2.2	Pattern	Stubs
[2]	50 × 50 × 1.6 FR4	1.88–2.5	26	2 SMP1304-04LF	4.54	Pattern	Stubs added on CPW
[4]	65 × 60 × 1 NELTECX	5.1–5.5 5.9–6.1	7.6 3.3	7 MA4SPS402	5.2	Polarization	Parasitic elements
[7]	45 × 50 × 1 Rogers 3850	2.2–2.53 2.97–3.71 4.51–6	13. 24 28	6 BAR64-02V	2.34	Frequency	Added Bowtie arms
[9]	30 × 40 × 0.44 Dimatix DMP-2831	1.5-4	83	2 SMP1302-079	2	Frequency	Added L & u radiators
[10]	75 × 75 × 0.76 Rogers4305B	2.3–3.2	36	4 HPND 3002	4.3	Pattern	Added Dipoles
[11]	65 × 65 × 0.508 Rogers 4003	2.34–2.55	8.7	2 SMV-2020	4.8	Pattern	Added Stubs
Proposed work	**40 × 28 × 0.1 Rogers ULTRAM 3850**	**(OFF-OFF) 3.5–5.5 (OFF-ON) 1.69–1.99 5.26–6.2 (ON-OFF) 1.72–2.10 5.12–6.4 (ON-ON) 1.8–2.36**	**44 16 16 19.8 18 26**	**2 BAR64-03V**	**3.5**	**Frequency and pattern**	**Added Circular ring to feed**

A comparative study with literature with respect to the current antenna model has been presented in Table 2. A moderate gain, efficiency, and hybrid reconfigurability are the main features for the designed antenna with compact dimension on commercially available material.

5. CONCLUSION

A compact flexible and conformal antenna on a liquid crystal polymer substrate is designed, analyzed, and presented in this work for off-body communication applications. The designed model is capable of switching with the help of BAR64 PIN diodes at different operating bands in the commercial communication applications of personal communications, wireless LAN, and industrial scientific and medical bands with measured impedance bandwidths of 43%, 25%, and 31%, respectively. The antenna shows pattern reconfigurability with a 30-degree orientation as per the switching conditions, and the evidence is presented and analyzed in this work. The designed model is flexible in nature and suitable for conformal wearable applications in the desired bands. The SAR average of 0.4 w/kg is observed at all switching positions, and the antenna is trustworthy as a suitable candidate for body area network applications. In addition, the proposed design strikes an advantageous equilibrium among ease of fabrication, cost-effectiveness, and practical integration into real-world applications. These considerations were pivotal in the assessment and evolution of this particular antenna configuration.

ACKNOWLEDGEMENT

We acknowledge KLEF-ALRC-R&D for the necessary prototyping and testing facility.

REFERENCES

[1] Aboufoul, T., C. Parini, X. Chen, and A. Alomainy, "Pattern-reconfigurable planar circular ultra-wideband monopole antenna," *IEEE Transactions on Antennas and Propagation*, Vol. 61, No. 10, 4973–4980, 2013.

[2] Jose, M. C., R. C. Devi, B. S. Sreeja, S. Meraline, and S. Radha, "A novel wideband pattern reconfigurable antenna using switchable parasitic stubs," *Microwave and Optical Technology Letters*, Vol. 61, No. 4, 1090–1096, 2019.

[3] Gao, G., B. Hu, L. He, S. Wang, and C. Yang, "Investigation of a reconfigurable dual notched UWB antenna by conceptual circuit model and time-domain characteristics," *Microwave and Optical Technology Letters*, Vol. 59, No. 6, 1326–1332, 2017.

[4] Singh, R. K., A. Basu, and S. K. Koul, "A novel reconfigurable microstrip patch antenna with polarization agility in two switchable frequency bands," *IEEE Transactions on Antennas and Propagation*, Vol. 66, No. 10, 5608–5613, 2018.

[5] Patel, K. and S. K. Behera, "Hybrid reconfigurable fractal antenna for multifunctional applications," in *2024 IEEE Asia-Pacific Microwave Conference (APMC)*, 1000–1002, Bali, Indonesia, 2024.

[6] Vitiello, R., G. Petraglia, F. Pascariello, G. Minatti, F. Caminita, and S. Maci, "Reconfigurable metasurface for electronic beam scanning antennas," in *2024 IEEE INC-USNC-URSI Radio Science Meeting (Joint with AP-S Symposium)*, 211–211, Florence, Italy, 2024.

[7] Jiang, R., D. Yu, L. Zhai, K. Xu, and J. Shi, "Frequency reconfigurable endfire antenna using coupled-type hybrid radiator with wide tuning range," *IEEE Antennas and Wireless Propagation Letters*, Vol. 23, No. 12, 4134–4138, 2024.

[8] Kaur, M., H. S. Singh, and M. Agarwal, "Design of a hybrid frequency and pattern reconfigurable antenna for 5G sub-6 GHz applications," in *2024 IEEE Wireless Antenna and Microwave Symposium (WAMS)*, 1–3, Visakhapatnam, India, 2024.

[9] Ibrahim, A. A., H. A. Mohamed, M. A. Abdelghany, and E. Tammam, "Flexible and frequency reconfigurable CPW-fed monopole antenna with frequency selective surface for IoT applications," *Scientific Reports*, Vol. 13, No. 1, 8409, 2023.

[10] Lakshmi, M., B. Madhav, H. Khan, and P. Kishore, "A frequency and pattern reconfigurable asymmetric ground antenna on flexible polyimide material for LTE, Wi-Fi, WLAN and fixed satellite applications," *Flexible and Printed Electronics*, Vol. 5, No. 2, 025007, 2020.

[11] Hussain, N., W. A. Awan, S. I. Naqvi, A. Ghaffar, A. Zaidi, S. A. Naqvi, A. Iftikhar, and X. J. Li, "A compact flexible frequency reconfigurable antenna for heterogeneous applications," *IEEE Access*, Vol. 8, 173 298–173 307, 2020.

[12] Ahmad, A., F. Arshad, S. I. Naqvi, Y. Amin, H. Tenhunen, and J. Loo, "Flexible and compact spiral-shaped frequency reconfigurable antenna for wireless applications," *IETE Journal of Research*, Vol. 66, No. 1, 22–29, 2020.

[13] Mahlaoui, Z., E. Antonino-Daviu, A. Latif, M. Ferrando-Bataller, and C. R. Peñafiel-Ojeda, "Frequency reconfigurable patch antenna using pin diodes with directive and fixed radiation pattern," in *2018 International Conference on Selected Topics in Mobile and Wireless Networking (MoWNeT)*, 1–3, Tangier, Morocco, 2018.

[14] Li, T., H. Zhai, X. Wang, L. Li, and C. Liang, "Frequency-reconfigurable bow-tie antenna for Bluetooth, WiMAX, and WLAN applications," *IEEE Antennas and Wireless Propagation Letters*, Vol. 14, 171–174, 2014.

[15] Yan, S. and G. A. E. Vandenbosch, "Radiation pattern-reconfigurable wearable antenna based on metamaterial structure," *IEEE Antennas and Wireless Propagation Letters*, Vol. 15, 1715–1718, 2016.

[16] Abutarboush, H. F. and A. Shamim, "A reconfigurable inkjet-printed antenna on paper substrate for wireless applications," *IEEE Antennas and Wireless Propagation Letters*, Vol. 17, No. 9, 1648–1651, 2018.

[17] Jin, G., M. Li, D. Liu, and G. Zeng, "A simple planar pattern-reconfigurable antenna based on arc dipoles," *IEEE Antennas and Wireless Propagation Letters*, Vol. 17, No. 9, 1664–1668, 2018.

[18] Chu, H. N., G.-Y. Li, and T.-G. Ma, "Planar pattern switchable antenna using phase reconfigurable synthesized transmission lines," *IEEE Antennas and Wireless Propagation Letters*, Vol. 17, No. 12, 2319–2323, 2018.

[19] Rezaeieh, S. A. and A. M. Abbosh, "Pattern-reconfigurable magnetoelectric antenna utilizing asymmetrical dipole arms," *IEEE Antennas and Wireless Propagation Letters*, Vol. 18, No. 4, 688–692, 2019.